Geometric calibration of thermal video frame scanners

Ahmed Mohamed Amin[a] and Gordon Petrie[b]

[a]University of the United Arab Emirates, Department of Civil Engineering,
Al Ain, United Arab Emirates.

[b]University of Glasgow, Department of Geography and Topographic Science,
Glasgow, G12 8QQ, Scotland, U.K.

ABSTRACT

Video imagers operating in the thermal infra-red part of the electro- magnetic spectrum have many different characteristics to those operating in the visible part of the spectrum. In particular, the highest performance thermal imagers incorporate a scanning mechanism which gives rise to a unique geometry. This paper outlines the main characteristics of thermal video frame scanners and gives an account of the methods devised and implemented by the authors to carry out the geometric calibration of these scanners. The results obtained from the calibration of seven frame scanners from different manufacturers are given. Analysis of these results shows that specific polynomial transformations can be derived and used successfully to remove the effects of the geometric distortions present in the video images obtained from thermal frame scanners.

1. INTRODUCTION

Thermal imaging systems, i.e. passive infra-red imaging systems, convert the thermal radiation of a scene (which is invisible to the human eye) into a visible image that can be viewed on a video monitor. Since the infra-red emission of the scene is used to generate the image and not its reflected solar radiation, its use allows day and night operation of the system. The ability to perceive images in total darkness and also the ability to penetrate smoke or mist and to identify camouflaged objects during daytime make these devices of great interest to *military users*. Indeed this interest has driven the development of these systems forward at a great rate. Thus thermal imaging devices producing video images are in widespread use (i) on airborne platforms - aircraft, RPVs, helicopters - as FLIR (Forward Looking Infra-red) devices for navigation and targeting; (ii) in armoured fighting vehicles - tanks, personnel carriers - for navigation, observation and fire control; (iii) as portable viewing devices for use by infantry for observation and reconnaissance and for artillery and mortar fire control; and (iv) as air defence alerting and tracking devices.[1]

The benefits of these thermal video imaging devices have also passed into the *civilian domain* where they are now being used routinely by a wide variety of users. These include (i) firefighting and rescue services to penetrate smoke; (ii) police forces and coastguards for surveillance, especially at night; (iii) the electricity supply industry for the monitoring of overhead transmission lines and generating plant and for cooling water studies; (iv) the building construction and services industry for the detection of heat loss from buildings and plant and for stress analysis in structures; and (v) medical applications such as the assessment of inflammatory conditions, vascular disorders and malignant diseases.[2]

From the videometrics point of view, the capability of making use of commonly available video recorders and display devices and the availability of video-based analytical equipment - frame stores, coordinate measuring devices, image processing systems, etc. - at comparatively inexpensive prices make the measurement of thermal video images quite a practical procedure. However the geometric characteristics and the calibration of these thermal video imaging devices are a matter for investigation. The results of such an investigation carried out at the University of Glasgow are reported in this paper.

2. CLASSIFICATION AND DESIGN CHARACTERISTICS OF THERMAL IMAGING DEVICES

Video imaging devices operating in the thermal infra-red region can be classified into three main groups:-

(i) *Vidicon-based devices* based on the pyro-electric vidicon which have been used extensively in industrial, medical and fire-fighting applications and have similar geometric characteristics to those of vidicon cameras

0-8194-1332-1/93/$6.00

operating in the visible art of the spectrum.

(ii) *Thermal cameras* employing focal plane arrays of photon detectors equivalent to the video cameras equipped with CCD areal arrays which are available for use in the visible part of the spectrum. These thermal infra-red detecting devices are now under intensive research and development, but are not as yet in any widespread industrial use. However a few are now being offered for sale by suppliers in various countries.

(iii) *Thermal frame scanners* using photon detectors in which the object space is scanned using optical elements such as oscillating mirrors and rotating polygons, often in combination with complex optical telescopes.

From the geometric point of view, all three types of thermal imager produce a discrete frame-type image, as distinct from the continuous strip images which are produced from optical-mechanical line scanners or pushbroom scanners employing linear arrays. However, while the first two types produce a planar image, the video frame scanner produces an image on a spherical surface arising from the scanning action which comprises scans by two optical elements (mirrors or polygons) operating at right angles to one another (Fig. 1 and Fig. 2). When used from airborne platforms, these basic geometries may be modified by platform motion during the time (1/50th second per field or 1/25th second for a full frame) over which the video image is acquired.

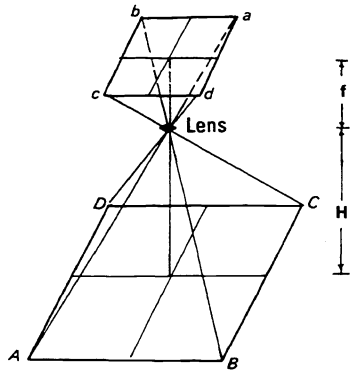

Fig. 1 - Planar Frame Image

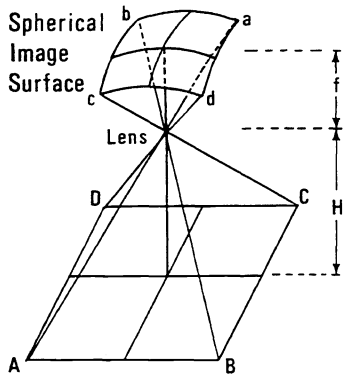

Fig. 2 - Spherical Frame Image

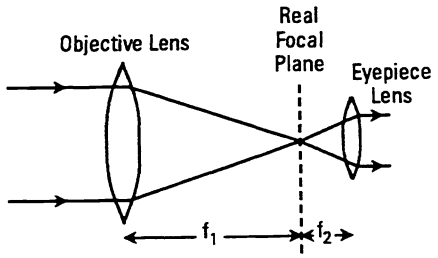

Fig. 3 - Afocal Telescope

2.1 Design and construction of thermal video frame scanners

Typically the video frame scanner will comprise (i) a telescope; (ii) a scanning mechanism; (iii) a relay lens; and (iv) a detector.

(i) Many video frame scanners use an *afocal telescope* (Fig. 3) consisting of a wide-aperture objective lens with a long focal length (f_1) and an eyepiece lens of a much shorter focal length (f_2), the two lenses being separated by the algebraic sum of these two focal lengths. The resulting magnification is the ratio of these two focal lengths. The radiation emerging from such an afocal telescope is supplied as a parallel or collimated bundle to the scanning mechanism. Afocal imagers have the advantage that they can achieve any required resolution through a suitable choice of telescope - albeit at the cost of a narrower field of view. [3]

Since glass does not transmit radiation at wavelengths (λ) beyond 2.5μm in the infra-red region, other less common materials have to be used for transmittive optical components. The most common are the semiconductor materials germanium (used in the λ= 8 to 14μm region) and silicon (used in the λ= 3 to 5.5μm waveband). Diamond anti-reflection coatings are much used on the outside surfaces of infra-red optical components, improving the scratch resistance and chemical durability of germanium optics.

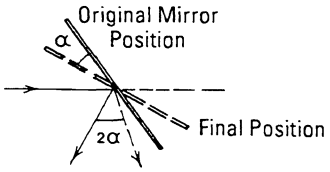

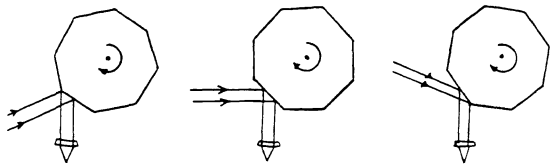

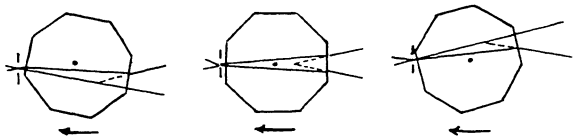

Fig. 4 - (a) Oscillating Plane Mirror

(b) Rotating Reflective Polygon

(c) Rotating Refractive Polygon

(ii) The *scanning mechanism* consists of two scanning elements - a line scanning element which carries out the scanning along each line of a video image on a pixel-by-pixel basis; and a frame scanning element which performs the line-by-line scan to form the field or frame. The most commonly used scanning elements are (a) the oscillating plane mirror; (b) the rotating reflective polygon; and (c) the rotating refractive polygon (Fig. 4) A combination of any two of these elements produces a complete scan of the object field in two dimensions. Fig. 5 shows the optical arrangement of the Barr and Stroud IR-18 employing an oscillating mirror and a 6 facet reflective polygon; Fig. 6 gives the optical layout of the AGA (now Agema) Thermovision 680 utilizing two rotating refractive/transmitting polygons; while Fig. 7 shows the coaxial arrangement with two reflective polygons, each with a different number of facets and rotating at a different rate as used in the Rank Pullin Controls (RPC) imager. Many reflecting surfaces, including both plane mirrors and rotating polygons, are machined from aluminium components and coated with thin films of gold for highest reflectivity in the infra-red region..

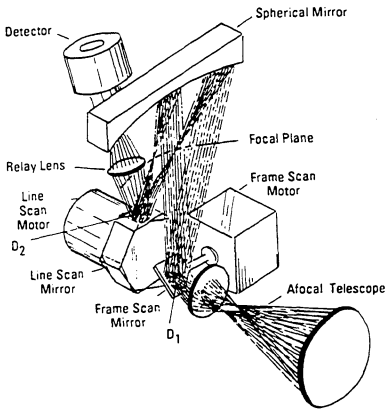

Fig. 5

Fig. 5 - Barr & Stroud IR - 18 Video Frame Scanner

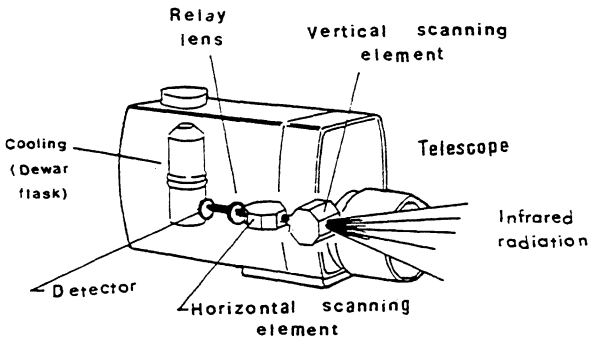

Fig. 6

Fig. 6 - AGA (Agema) Thermovision Model 680

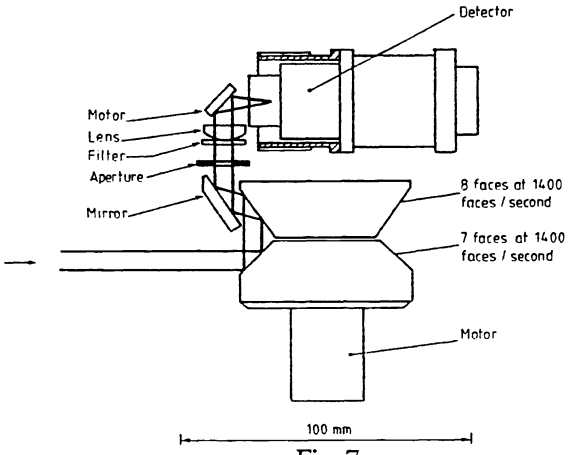

Fig. 7

Fig. 7 - Rank Pullin Controls (RPC) Imager

(iii) The *relay lens* or detector optics, which may comprise several lens elements, take the radiation emerging from the scanner optical system and focus it on to the detector array.

(iv) The most widely used *detectors* in video frame scanners are indium antimonide (InSb) and lead selenide (PbSc) in the λ= 3 to 5.5μm region and cadmium mercury telluride (CMT or HgCdTe) and lead tin telluride (LTT) in the λ= 8 to 14μm region. Cooling of the detectors to temperatures of about 80°K is a requirement for almost all of the materials used to detect radiation in the λ= 8 to 14μm band to ensure noise-free operation and adequate sensitivity to small temperature differences. This is done using compressed (high pressure) air and a Joule-Thomson mini cooler or an integral Stirling cooler. Those detectors operating in the middle infra-red band (λ= 3 to 5.5μm) operate at around 195°K and use thermo-electric coolers based on the Peltier effect. A much used form of detector is the so-called SPRITE detector, the name being an acronym formed from the words Signal PRocessing In The Element. This consists of a strip of n- type CMT which performs the same basic function as a row of serial detectors, with the time delay and integration (TDI) procedure taking place in the material itself.

Most modern frame scanners feature *serial/parallel scanning* based on the use of an array of detectors (Fig. 8). This combines the practical advantages of the slower speed of the parallel scanning techniques with the good signal-to- noise ratio produced by serial scanning, as for example using the SPRITE detector. The full video field or frame is then generated by scanning the object in a number of swaths across the field of view.

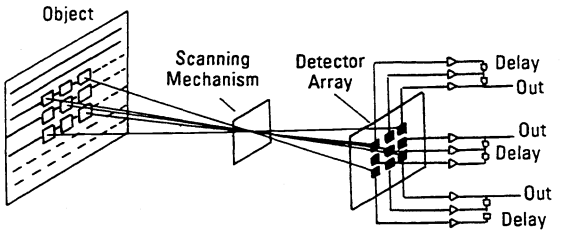

Fig. 8 - Serial / Parallel Scanning using an array of detectors

From the above description, it will be seen, that compared with vidicon and CCD areal array cameras, equipped typically with a fixed 3 element objective lens, the video frame scanner has a much more complex optical system, including a scanning mechanism comprising both line and frame scanning elements besides the fixed optical elements of the afocal telescope and the relay lens system placed in front of the detector array. It is not practical to carry out calibration of each of these individual elements of the frame scanner. Instead a geometric calibration of the system as a whole would appear to be a more practical proposition.

2.2 Geometry of video frame scanner images

The basically spherical surface on which the frame scanner image is produced has already been given in Fig. 2 with all the points on the image equidistant from a single perspective centre (O). This will apply if the scanner is used in a stationary mode where the object is also stationary. If the scanner is operated from an airborne platform which is in motion, then various displacements will be added to the basic geometric distortion pattern of the scanner itself. These include the effects of the platform's forward motion during the time (1/25s = 40ms) during which a complete video frame (of two fields) is scanned. To these would be added the effects of the platform tilts and changes in tilt also being experienced during the exposure time of a single frame. However these will not be dealt with here since this paper is concerned solely with the geometric calibration of the scanner itself.

Since there is no target plate or focal plane present in a video frame scanner of the type present in vidicon or areal array cameras, there is no possibility of using a method such as an etched reseau grid as has been done with vidicon based devices. [4,5,6,7] Furthermore any array of calibration targets located in the object space must exhibit a good thermal emissivity that ensures a good contrast between the images of these targets and their background.

3. DESIGN AND MANUFACTURE OF THE CALIBRATION TARGET PLATE

Having regard to these considerations, a special *target plate* (Fig. 9) was designed and manufactured for the calibration of video frame scanners operating in the thermal infra-red region. This consists of a very thin (0.2mm thick) stainless steel plate, 45x30cm in size, with 150 individual x-shaped crosses chemically etched into its surface to form voids. The arms of each of these 150 target crosses are each 14mm in diagonal length and each cross arm has a thickness of 2mm. The crosses are arranged in a symmetrical pattern of 10 rows by 15 columns with a 3cm spacing between them. In addition, 24 resolution targets (copied from a television test card) were also etched into the plate to test the scanner resolution in both the horizontal and vertical directions.

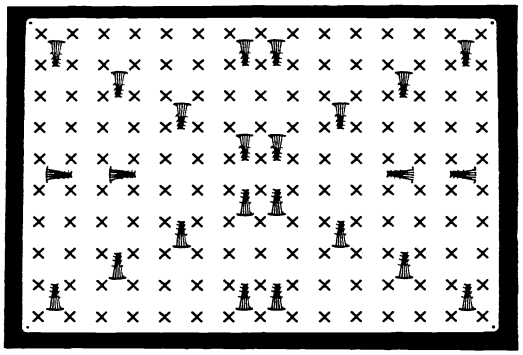

Fig. 9 - Calibration Target Plate with 150 x-shaped crosses

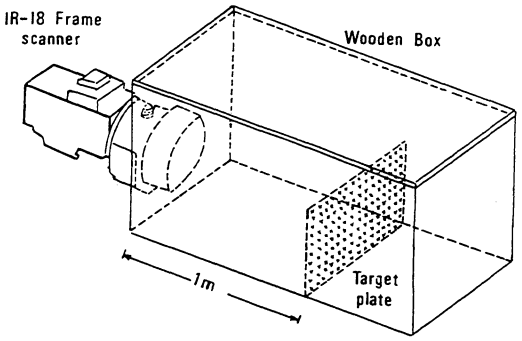

Fig. 10 - Target Plate mounted in shielding box

This thin stainless steel plate was then bonded on to a glass plate, both to add rigidity to the target and to provide a very high contrast between the target crosses and the background steel plate. This results from the very high thermal emissivity factor of glass relative to that of the steel plate (0.95 v 0.06). When heated slightly with a hot air gun, the crosses showed up strongly and sharply as white images against the almost black background. The glass plate was painted with a heat resistant paint on the side against which the steel plate was bonded on to the glass, so that the heat of the glass was not transferred quickly to the steel plate. The output images from each frame scanner tested were collected on a U-matic VTR over a period of 20 minutes. From this record, several frames could be selected at intervals and measured to see if the distortion pattern varied with time.

The target plate was itself calibrated at the National Engineering Laboratories (NEL) using a Ferranti monocomparator equipped with linear encoders having 1μm resolution. The 150 crosses were measured twice, forward and backward, and the mean value adopted for each point. The precision (m_x=m_y) of measuring the crosses was ±20μm.

To prevent emission or reflections from other ambient bodies, the calibrated target plate was mounted in a wooden box (Fig. 10) which had its interior walls coated with a special absorbent black paint to cut down any emitted or reflected radiation occurring within the box. The distance between the frame scanner and the target plate varied between 70cm and 2.5m depending on the magnification (and therefore the angular coverage) of the particular telescope used. Thus for example with the Barr & Stroud IR-18 frame scanner, the respective distances were 70cm (with a 1x magnification telescope), 1.0m (with 1.5x magnification) and 2.25m (with 6x magnification).

4. MEASUREMENT OF THE VIDEO IMAGES OF THE CALIBRATION PLATE

The images of the crosses on the target plate were measured on a *video- based monocomparator* (Fig. 11) consisting of the following elements:-

(i) a Sony U-matic *VTR*;

(ii) a FOR.A *video frame memory* (512x512 pixels) which accepts the analogue video image data from the VTR and converts it to digital form for storage in the frame store;

(iii) a FOR.A *video position analyser* (VPA) which is connected to the frame store and allows direct measurement of the recorded target crosses by an operator using a cursor under the control of two control knobs. The measured x and y coordinates are expressed in pixel count values;

(iv) a standard monochrome video display *monitor*.

Fig. 11 - Video-based monocomparator

An important point to mention is that the measurements take place wholly within the digital frame store, so that any distortions present on the monitor screen do not affect the coordinate measurements. The accuracy of the video monocomparator was also tested using a FOR.A *video scaler* which generates a very accurate grid electronically. Using this device, the internal accuracy (m_x=m_y) was found to be ±0.1 pixel.

Scanner	RMSE in pixels	
	m_x	m_y
IR-18	0.35	0.25
TICM	0.40	0.48
RPC	0.50	0.40
AGA	1.20	0.90

Table I - Precision of Measuring the Target Plate Coordinates on the Video Monocomparator

Five video images of the target plate were measured in the video monocomparator for each of the four frame scanners tested - the Barr & Stroud IR-18, the GEC Avionics TICM II, the Rank Pullin Controls RPC and the AGA (Agema) Thermovision 782. The precision of measurement of the cross images for each of the four scanners tested is given in Table I. These correspond roughly to the respective resolution values of these scanners. The results comparing the measured coordinate values of the recorded image positions of the target crosses against their known or calibrated coordinate values using a linear conformal (similarity) transformation produces the same distinctive symmetrical pattern with all four scanners. Two representative examples are shown in Figs. 12 and 13. These represent the basic geometric distortion pattern produced by the instrument's optical and scanning system before any attempt is made to correct for this.

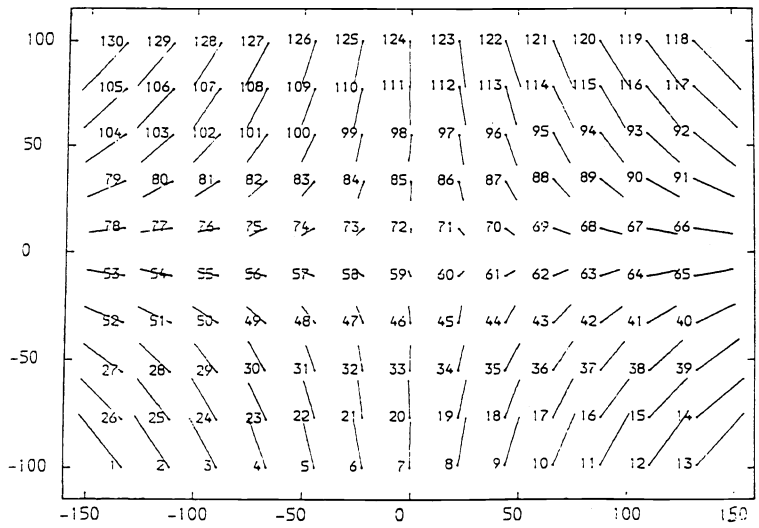

Fig. 12 - Vector Plot after application of a linear conformal transformation showing the basic geometric distortion present in the image taken by the Barr & Stroud IR-18 video frame scanner.

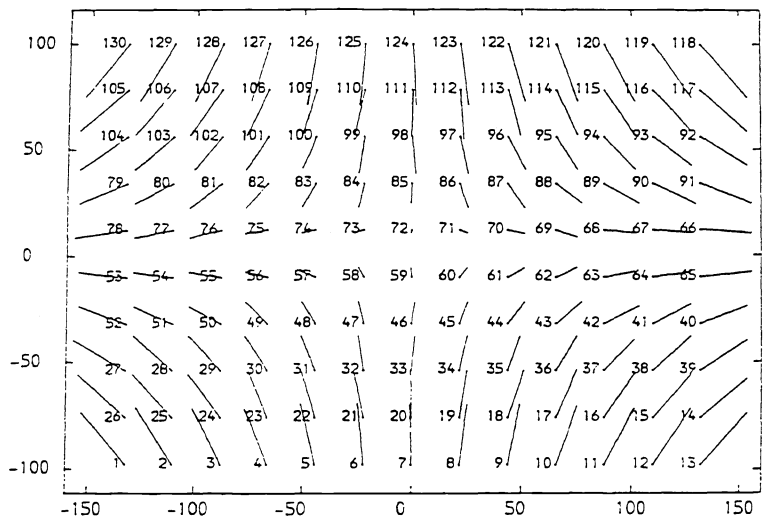

Fig. 13 - Vector Plot after application of a linear conformal transformation showing the basic geometric distortion present in the image taken by the Rank Pullin Control (RPC) video frame scanner.

5. ANALYSIS OF RESULTS FROM THE CALIBRATION PROCEDURE

The results from the calibrations were analysed using a general 25-term polynomial transformation having the form:-

$$x' = a_0 + a_1x + a_2y + a_3xy + a_4x^2 + a_5y^2 + a_6x^2y^2 + a_7x^2y + a_8xy^2 + a_9x^3 + a_{10}y^3 + a_{11}x^3y + a_{12}xy^3 + a_{13}x^3y + a_{14}x^2y^3 + a_{15}x^3y^3 + a_{16}x^4 + a_{17}y^4 + a_{18}x^4y + a_{19}xy^4 + a_{20}x^4y^2 + a_{21}x^2y^4 + a_{22}x^4y^3 + a_{23}x^3y^4 + a_{24}x^4y^4$$

$$y' = b_0 + b_1x + b_2y + \text{----------} + b_{24}x^4y^4 \qquad (1)$$

This was implemented as a FORTRAN program running on an ICL/VME mainframe computer, in such a way that any specific set of terms can be used to carry out the transformation between the measured and known values of the coordinates of the crosses. The results were presented both as a set of tabular numerical values and in the form of a graphical plot showing the size and direction of the error vector at each measured position. A summary of the results are given in Table II below. These comprise the average of the five sets of measurements carried out on different frames for each of the four video frame scanners tested. The table contains the results using the polynomial transformation only as far as the 13th term, since the use of higher order terms in the polynomials than this showed no improvement in the results obtained from any of the scanners tested.

Table II - Calibration Results for the Four Frame Scanners Showing the Effects of Individual Parameters of the Transformation

Scanner	IR - 18		RPC		TICM II		AGA	
R.M.S.E. (pixels)	m_x	m_y	m_x	m_y	m_x	m_y	m_x	m_y
Linear Conformal	5.80	7.51	6.75	8.83	6.75	8.92	6.75	8.82
Affine	**0.67**	**0.50**	**0.50**	**0.62**	**0.73**	**2.68**	**0.57**	**0.60**
4 - term xy	0.65	0.48	0.50	0.62	1.73	2.68	0.57	0.60
5 - term x^2	0.65	0.48	0.49	0.62	1.73	2.68	0.56	0.59
6 - term y^2	0.63	0.46	0.50	0.62	1.73	2.67	0.56	0.59
7 - term x^2y	0.63	**0.39**	0.50	**0.46**	1.73	**0.74**	0.56	**0.53**
8 - term xy^2	**0.47**	0.39	**0.45**	0.46	**0.77**	0.74	**0.51**	0.53
9 - term x^2y^2	0.46	0.39	0.45	0.46	0.77	0.74	0.52	0.53
10 - term x^3	**0.34**	0.39	**0.37**	0.46	**0.47**	0.74	**0.45**	0.53
11 - term y^3	0.34	**0.30**	0.37	**0.41**	0.46	**0.54**	0.45	**0.46**
12 - term x^3y	0.33	0.30	0.37	0.41	0.47	0.54	0.45	0.46
13- term xy^3	0.33	0.30	0.37	0.41	0.47	0.54	0.45	0.46

Table III shows the results obtained using afocal telescopes of *different magnification* (1x, 1.5x and 6x) fitted to the IR-18 scanner. The pattern of distortion remained the same, albeit with slightly different magnitudes, while the polynomial terms which had significant effect in reducing the distortion were again those shown in Table II above.

Table III
Calibration Results for the Barr & Stroud IR - 18 Frame Scanner with Telescopes of Different Magnification

Magnification	1x mag		1.5x mag		6x mag	
R.M.S.E.	m_x	m_y	m_x	m_y	m_x	m_y
Linear Conformal	5.80	7.51	5.80	6.50	6.74	7.85
Affine	**0.67**	**0.50**	**0.65**	**0.56**	**0.71**	**0.57**
4 - term xy	0.65	0.48	0.65	0.56	0.71	0.57
5 - term x^2	0.65	0.48	0.65	0.56	0.71	0.57
6- term y^2	0.63	0.47	0.65	0.55	0.71	0.57
7 - term x^2y	0.63	**0.39**	0.64	**0.45**	0.70	**0.45**
8 - term xy^2	**0.47**	0.39	**0.48**	0.45	**0.52**	0.45
9 - term x^2y^2	0.47	0.39	0.48	0.45	0.52	0.45
10 - term x^3	**0.34**	0.39	**0.36**	0.45	**0.37**	0.45
11 - term y^3	0.33	0.30	0.36	0.36	0.37	0.34
12 - term x^3y	0.33	0.30	0.36	0.36	0.37	0.34
13 - term xy^3	0.33	0.30	0.36	0.36	0.37	0.34

Inspection of the results given in Tables II and III show that the application of a simple *affine transformation* of the form

$$x' = a_0 + a_1x + a_2y$$
$$y' = b_0 + b_1x + b_2y \qquad (2)$$

which removes the difference in scale between the x and y directions and any lack of orthogonality between the x and y axes, caused a dramatic reduction in the magnitude of the distortion present in the test images from all four scanners. Further inspection of the table shows that the other terms having a significant effect in the reduction of the geometric distortion were those in xy^2 and x^3 in the x-direction only and those in x^2y and y^3 in the y-direction only. Thus on the basis of the results obtained from the above tests, two *specific transformation polynomials* having the form

$$x' = a_0 + a_1x + a_2y + a_3xy^2 + a_4x^3$$
$$y' = b_0 + b_1x + b_2y + b_3x^2y + b_4y^3 \qquad (3)$$

could be recommended to compensate for the effects of geometric distortion when measuring video frame scanner imagery. The remaining distortion present in the images would then be at a satisfactory and usefully low level (m_x=m_y= 0.3 to 0.5 pixel).

This appeared to provide a fairly simple and effective method of dealing with the geometric distortions inherent in thermal frame scanner imagery and indeed the present authors have used the method very effectively in carrying out further tests of the accuracy of airborne scanner imagery taken over test fields in the Glasgow area.

6. CALIBRATION TESTS CARRIED OUT ON THE LATEST GENERATION OF FRAME SCANNERS

However a new generation of video frame scanners has appeared recently, the majority showing considerably improved resolution due to improvements both in lens design and manufacture, and in the minimum resolvable temperature difference (MRTD) measured by the detector. Another feature of these new thermal video frame scanners has been the redesign of the scan mechanisms both with a view to an improvement in their efficiency and to a reduction in their size and weight, which in turn leads to more compact and lighter imager. Other improvements have been made to the system electronics including an embedded microprocessor to allow monitoring of signals, image processing and digital recording of the images.

Further calibration tests have therefore been carried out on some of these new scanners using the same technique as described above. The instruments tested so far have included the Agema Thermovision 1000 and 210 models and the Thorn EMI Multi Role Thermal Imager (MRTI). The Model 210 is a hand held frame scanner, only slightly larger than a 35mm film camera, with a limited format size and dynamic range. The Model 1000 and the MRTI are state-of-the art frame scanner systems with dual fields of view (narrow and wide angle), large dynamic range and output to various video standards (EIA, CCIR, RGB, etc.). The results of these recent tests are given in Table IV.

Table IV
Calibration Results for the Three Recent Frame Scanners Showing the Effects of Individual Parameters of the Transformation

Scanner	Agema 1000		Agema 210		Thorn EMI MRTI	
R.M.S.E. (pixels)	m_x	m_y	m_x	m_y	m_x	m_y
Linear Conformal	1.38	1.16	8.43	8.84	6.79	7.40
Affine	**0.78**	**0.68**	**0.60**	**0.66**	**0.34**	**0.38**
4 - term xy	0.76	0.67	0.60	0.66	0.34	0.36
5 - term x^2	0.76	**0.55**	**0.40**	0.66	0.34	0.36
6 - term y^2	0..75	0.53	0.38	**0.49**	0.33	0.36
7 - term x^2y	0.75	**0.49**	0.38	0.49	0.33	0.36
8 - term xy^2	**0.60**	0.49	0.38	0.49	0.33	0.35
9 - term x^2y^2	0.60	0.49	0.38	0.48	0.32	0.35
10 - term x^3	**0.33**	0.49	0.35	0.48	0.32	0.35
11 - term y^3	0.33	**0.26**	0.35	0.47	0.32	0.35
12 - term x^3y	0.32	0.26	0.35	0.47	0.32	0.35
13- term xy^3	0.32	0.26	0.35	0.47	0.32	0.35

It will be seen that the results differ somewhat from those shown in Tables II and III.

6.1 Calibration test of the Agema Thermovision 1000

In the case of the *Agema Thermovision 1000*, while the same four terms - xy^2 and x^3 in the x-direction and x^2y and y^3 in the y-direction are significant in reducing the geometric distortion, the term in x^2 was also significant in this respect. While the multi-element objective and the relay or detector optical train may have some influence in this matter, it seems much more probable that the source of this additional geometric disturbance is the redesigned scanner system (Fig. 14). The first part of this system comprises an oscillating plane mirror (imparting the vertical scan motion), a fixed plane mirror and an aspheric mirror, followed by a third plane mirror which projects the radiation on to a rotating polygon which carries out the horizontal scan motion. This reflects the radiant energy on to a second aspheric mirror and then on to a final mirror which reflects the radiation back on to the opposite face of the rotating polygon. From there, the radiation passes through a field-stop into the relay optics of the detector unit. In this way, the complex scanning unit consists solely of reflective optics which allows relative ease of optical alignment of the system during the manufacture and assembly of the unit.

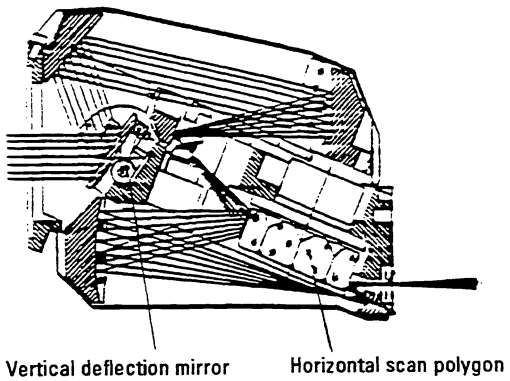

Fig. 14 - Agema Thermovision 1000 Scanning Mechanism

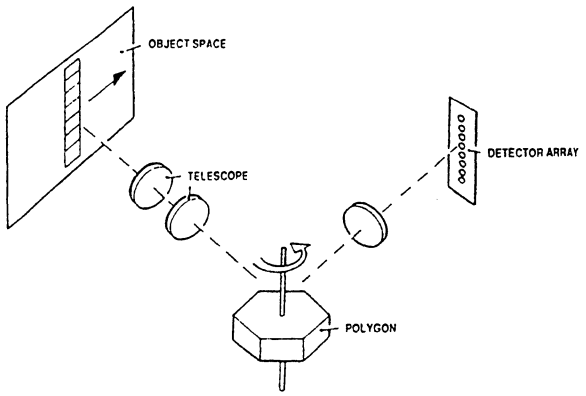

Fig. 15 - Agema Thermovision 210 Scanning Mechanism

6.2 Calibration test of the Agema Thermovision 210

The Thermovision 210 employs lead selenide (PbSe) detectors sensitive to radiation in the middle infra-red region (λ=3 to 5.5μm) and cooled to an operating temperature of 195°K using a Peltier cooler. This small hand-held scanner, has a limited format size of about 250 lines (although the output signal is TV compatible). It also features a very simple scanning mechanism (Fig. 15) in which a mirror sweeps the incoming radiation from the objective lens sideways on to a 48 detector linear array mounted vertically in the camera to produce a single field. With the use of a six sided polygon, successive sweeps of the mirror surface generate the remaining lines of the TV/video frame.

The results of the calibration given in Table IV show that the significant terms for removal of geometric distortion using the polynomial transformation (after the application of the affine transformation) are x^2 in the x-direction and y^2 and y^4 in the y-direction. While the x^2 term can be accounted for quite simply by the polygon mirror sweep motion in the x-direction, the source of the distortion in the y-direction is less clear and at present awaits further clarification by the manufacturer.

6.3 Calibration test of the Thorn EMI MRTI

As can be seen in Table IV, after the application of the initial affine transformation, the r.m.s.e. values fell immediately to m_x=m_y= 0.35 to 0.4 pixel. Furthermore the vector plot of the residual distortions showed a wholly random (i.e. non-systematic) pattern. The application of all the further terms in the polynomial transformation had virtually no effect.

Investigation of the optical arrangement revealed a single but ingenious design (Fig. 16). In this, the image generated by the scanning pattern within the scanner for the object field using an oscillating plane mirror and a rotating polygon is recorded on a detector array of 23 elements. The twenty-three outputs from the detector elements are amplified and processed by the scanner's electronics module to produce video outputs which are applied to the 23 elements of an LED array. The image produced via the LED array then travels via another frame scan mirror and the rotating polygon to be viewed either directly (i.e. visually) by the operator or indirectly by converting the LED light input to a CCIR compatible television signal which can be viewed on a standard video monitor. In this way, the geometric distortion present in the image produced by the scanning mechanism is compensated for through the use of an equivalent optical path working in the reverse direction. A single rocking frame carries the two frame scan mirrors which are rocked simultaneously via a cam, while the line scan polygon is continuously rotating using a drive motor in conjunction with a gear train.

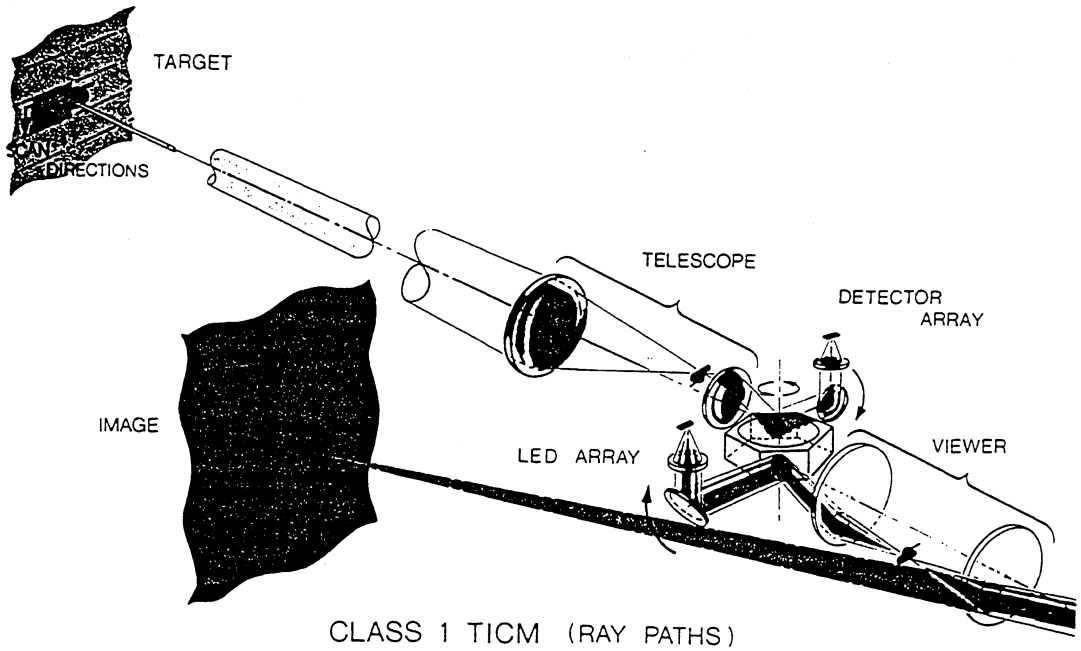

Fig. 16 - Thorn EMI Multi-Role Thermal Imager (MRTI) optical arrangement

6.4 Summary

The results of the geometric calibration tests carried out in the work described above show that a satisfactory and useful geometric calibration of video frame scanners can be carried out using the equipment and procedures outlined above. Furthermore the majority of video frame scanners can have quite simple polynomial transformations applied to the measurements made on the video image to reduce their geometric distortions to a quite minimal level. However the testing of certain new scanners has revealed new image geometries which are substantially different to the well established pattern encountered with the previous generation of these scanners. This simply reinforces the need for geometric calibration of thermal frame scanners if the images are to be used for videometric analysis.

7. ACKNOWLEDGEMENTS

It is a real pleasure to acknowledge the very full cooperation which was given by the various manufacturers - Barr & Stroud, Rank Taylor Hobson, Rank Pullin Controls, AGA/Agema and Thorn EMI - in making available their respective frame scanners and the facilities of their laboratories for the tests reported in this paper. The National Engineering Laboratories (NEL) at East Kilbride near Glasgow were also most cooperative in making available their Ferranti monocomparator for the target plate calibration. In addition, the staff of Photofabrication in Huntingdon were most helpful in tackling the manufacture of the target calibration plate, a task which was far from routine for them to execute.

8. REFERENCES

1. K. Venables, "Thermal Imaging," Chapter 7 in *Principles of Modern Optic Systems*, Vol. II, Artech House, pp. 201-220.

2. S. G. Burney, T. L. Williams and C. H. Jones (Editors), "*Applications of Thermal Imagery*", Adam Hilger, 1988.

3. A. P. Davis and A. H. Lettington, "Principles of Thermal Imaging", Chapter 1 in *Applications of Thermal Imaging*, Adam Hilger, pp. 1-34., 1988.

4. K. W. Wong, "Geometric calibration of television images for photogrammetric applications," *Civil Engineering Studies, Photogrammetric Series*, No. 16, University of Illinois, 1968.

5. K. W. Wong, "Photogrammetric quality of television images," *Civil Engineering Studies, Photogrammetric Series*, No. 17, University of Illinois, 1968.

6. K. W. Wong, "Fidelity of space TV," *Photogrammetric Engineering*, Vol. 36, No. 5, pp 491-497, May 1970.

7. K. W. Wong, "Geometric analysis of the RBV television system," *Civil Engineering Studies, Photogrammetric Series*, No. 35, University of Illinois, 1972.

8. G. Petrie, "The philosophy of digital and analytical photogrammetric systems," *Proceedings of the 39th Photogrammetric Week, University of Stuttgart*, pp. 53-68, Sept. 1983.